# Topological superconductivity from first principles. I. Shiba band structure and topological edge states of artificial spin chains

Bendegúz Nyári,[1,2] András Lászlóffy,[3] Gábor Csire,[4,5] László Szunyogh,[1,2] and Balázs Újfalussy[3]

[1]*Department of Theoretical Physics, Institute of Physics, Budapest University of Technology and Economics, Műegyetem rkp. 3., HU-1111 Budapest, Hungary*

[2]*HUN-REN-BME Condensed Matter Research Group, Budapest University of Technology and Economics, Műegyetem rkp. 3., HU-1111 Budapest, Hungary*

[3]*HUN-REN Wigner Research Centre for Physics, Institute for Solid State Physics and Optics, H-1525 Budapest, Hungary*

[4]*Materials Center Leoben Forschung GmbH, Roseggerstraße 12, 8700 Leoben, Austria*

[5]*Catalan Institute of Nanoscience and Nanotechnology (ICN2), CSIC, BIST, Campus UAB, Bellaterra, Barcelona 08193, Spain*

(Received 11 April 2023; accepted 2 October 2023; published 23 October 2023)

Magnetic chains on superconductors hosting Majorana zero modes (MZMs) have attracted a great deal of interest due to their possible applications in fault-tolerant quantum computing. However, this is hindered by the lack of a detailed, quantitative understanding of these systems. As a significant step forward, we present a first-principles computational approach based on a microscopic relativistic theory of inhomogeneous superconductors applied to an iron chain on the top of Au-covered Nb(110) to study the Shiba band structure and the topological nature of the edge states. Contrary to contemporary considerations, our method enables the introduction of quantities indicating band inversion without fitting parameters in realistic experimental settings, holding thus the power to determine the topological nature of zero-energy edge states in an accurate *ab initio* based description of the experimental systems. We confirm that ferromagnetic Fe chains on an Au/Nb(110) surface do not support any separated MZM; however, a broad range of spin-spirals can be identified with robust zero-energy edge states displaying signatures of MZMs. For these spirals, we explore the structure of the superconducting order parameter, shedding light on the internally antisymmetric triplet pairing hosted by MZMs. We also reveal a twofold effect of spin-orbit coupling: although it tends to enlarge the topological phase regarding spin spiraling angles, it also extends the localization of MZMs. Due to the presented predictive power, our work fills a big gap between experimental efforts and theoretical models while paving the way for engineering platforms for topological quantum computation.

DOI: 10.1103/PhysRevB.108.134512

## I. INTRODUCTION

Topological superconductivity is an exotic state of matter where the condensate of Cooper pairs of electrons spontaneously breaks the U(1) gauge symmetry and simultaneously exhibits a nontrivial topological gap structure [1,2]. Although there may well be materials that develop intrinsic topological superconductivity providing natural platforms for Majorana zero modes (MZMs) [3–12], the real breakthrough—that has created a great number of routes to such platforms—was the realization that one can create topological superconductivity based on artificial heterostructures [13–51]. Due to the bulk-edge correspondence principle [1], one-dimensional topological superconductivity is manifested in zero-energy edge states: the renowned Majorana zero modes. These states have drawn a significant interest of the scientific community since MZMs may have applications for topological quantum computing [52–54]. However, MZMs in superconducting heterostructures are still elusive because it is very difficult to uniquely identify them experimentally. Several promising scanning tunneling microscopy (STM) experiments have been performed on various systems, which show peaks in the differential conductivity at zero energy [55–58] in the superconducting gap of the host. However, this does not impose strict evidence that the observed states at the end of the chain are indeed the long-sought MZMs, and further information about the nature of these peaks is difficult to obtain.

To address this problem, we developed a first-principles based computational approach serving as a template for detailed analysis of different MZM platforms. This is allowed by the Green's-function-based solution of the Kohn-Sham-Dirac-Bogoliubov–de Gennes (KSDBdG) equations [59,60]. On the one hand, it has been demonstrated previously that many aspects of STM experiments are reproducible by such calculations [60–63], while on the other hand, it allows us to calculate other quantities, such as spin-polarization and the superconducting order parameter (OP) [64], which are important to understand the nature of these states. Furthermore, some of their properties can be further explored and tested by computational experiments which go beyond the capabilities of conventional experimental techniques.

In what follows, we show first-principles calculations performed for Fe chains on top of a superconducting Nb(110) host with a single epitaxial Au overlayer, as introduced in Ref. [65], in the superconducting state, where relativistic effects, superconductivity, and the complex electronic structure are treated on the same level. Based on previous simple model calculations, there are two essential ingredients for the formation of MZMs in spin chains proximitized with *s*-wave

 

superconductors, namely strong Rashba spin-orbit coupling (SOC) [14,15] or a noncollinear spin structure, such as a spin spiral [20,47,66–68], both inducing $p$-wave pairing [69] and hence topological superconductivity. One idea, which was realized in a recent experiment, is to cover the surface of an $s$-wave superconductor with a single atomic layer of a heavy metal [65]. This has the advantage of keeping the relatively large superconducting gap of Nb while simultaneously enhancing the SOC in the system. However, in spite of the enhanced SOC, there was no experimentally observable minigap in the system. Further theoretical investigations revealed [65] that, by forcing the system into a 90° spin-spiral state, it is possible to open up a minigap hosting zero-energy end states. This previously obtained finding just asks for the application of first-principles methods described in Sec. II, which can further substantiate the topological classification of these states and provide practical guidance for further experiments. In Sec. III, by considering a wide range of spiraling angles, we make quantitative predictions for the local density of states (LDOS) as described in Ref. [60], and by changing the spiraling angle we show that it drives the system through topological phase transitions. At these points, the minigap closes and the zero-energy states appear or disappear. We also show how this picture changes if we utilize the capability of our method to artificially scale the SOC. In an attempt to validate the developed method, we verify the expected result that in a ferromagnetic chain without spin-orbit coupling there is no topological superconductivity and MZMs [20]. In Sec. IV we shall study the spatial distribution of the zero-energy peak, which reveals a twofold effect of SOC: although it tends to enlarge the topological phase regarding spin spiraling angles, it also extends the localization of MZMs. Our model makes it possible to explore quantities that are beyond the current capabilities of experiments to measure. The superconducting OP [64] belongs to this category, and in Sec. V we discuss that it has a more complex structure (involving both spin singlet and triplet parts) than in the well-known prototype models [20,25,31,33,44,67,68,70,71] for Majorana zero modes. We identify that the structure of the superconducting OP (more precisely, its energy resolution, introduced later) can serve as an indicator of band inversion and thus topological superconductivity. Finally, in Sec. VI we further analyze the topological nature of the minigap by illustrating the appearance of band inversion based on the spin singlet OP and the quasiparticle charge density of states. Remarkably, quantities being antisymmetric in energy with respect to the Fermi level offer a possible route to identify the topological nature of the gap in STM experiments.

## II. FIRST-PRINCIPLES-BASED TREATMENT OF AN ARTIFICIAL SPIN CHAIN ON A SUPERCONDUCTING HOST

The density functional theory yielding Kohn-Sham equations has been proven to successfully describe material-specific properties. The concept of superconductivity can be introduced into this theory by treating the superconducting OP as an additional (so-called) anomalous density [72]. Such a generalization of Kohn-Sham equations leads to the following KSDBdG Hamiltonian written in Rydberg units:

$$H_{\mathrm{DBdG}} = \begin{pmatrix} H_D & \Delta_{\mathrm{eff}} \\ \Delta_{\mathrm{eff}}^{\dagger} & -H_D^{*} \end{pmatrix}, \tag{1}$$

where $H_D(\vec{r}) = c\vec{\boldsymbol{\alpha}}\vec{p} + (\boldsymbol{\beta} - \mathbb{I}_4)c^2/2 + [V_{\mathrm{eff}}(\vec{r}) - E_F]\mathbb{I}_4 + \vec{\boldsymbol{\Sigma}}\vec{B}_{\mathrm{eff}}(\vec{r})$, with $\vec{\boldsymbol{\alpha}} = \boldsymbol{\sigma}_x \otimes \vec{\boldsymbol{\sigma}}$, $\boldsymbol{\beta} = \boldsymbol{\sigma}_z \otimes \mathbb{I}_2$, $\vec{\boldsymbol{\Sigma}} = \mathbb{I}_2 \otimes \vec{\boldsymbol{\sigma}}$, $\vec{\boldsymbol{\sigma}}$ denotes the Pauli matrices, and $\mathbb{I}_n$ is the identity matrix of order $n$. $V_{\mathrm{eff}}(\vec{r})$ and $\vec{B}_{\mathrm{eff}}(\vec{r})$ are the effective potential and the exchange field, respectively. $\Delta_{\mathrm{eff}}(\vec{r})$ is the effective $4 \times 4$ pairing potential matrix due to the four-component Dirac spinors. The KSDBdG equations shall be solved self-consistently by assuming that the superconducting host has isotropic $s$-wave spin-singlet pairing as described by BCS theory [73]. Computational details are given in the Appendix, while more details of the formalism can be found in the Supplemental Material [74]. The central quantity of our approach, the Green's function, is obtained from the generalized multiple scattering theory in a self-consistent way. The great advantage of such a Green's-function technique [75] is the exact treatment of semi-infinite geometries (hence the superconducting host) together with the embedding of magnetic chains (see note 1 of the Supplemental Material [74]). In this way, involving both the orbital and spin degrees of freedom, we can properly account for the microscopic complexity in the superconducting state of the studied iron nanowire placed on an Au monolayer grown epitaxially on the (110) surface of niobium.

For each site of the chain, the method yields the local Green's function matrix $\{G^{nn,ab}_{Ls,L's'}(\varepsilon)\}$ (see note 1 of the Supplemental Material [74]), where $n$ denotes the sites of the chain; $L = (l, m)$ and $L' = (l', m')$ are composed angular momentum indices; $s, s'$ are the spin indices; and $a, b$ corresponds to either the electronlike or the holelike part of the Green's function. This quantity contains all information about the superconducting ground state involving the description of all the pairing states present in the system. Hence, this allows the calculation of the LDOS and the energy-resolved OP related to different pairing states, as defined later. Such an approach has two major advantages compared to effective models such as the tight-binding approximation. First, there is no further need to fit the electronic structure with artificial tight-binding parameters, which in turn allows for computational experiments with spin chains more easily. Second, it is crucial to have a proper model of the (semi-infinite) superconducting host if one aims to predict quantitatively the localization length of MZMs. The problem of insufficient modeling of the semi-infinite host appears in most tight-binding approximations. These calculations resulted in an unrealistic gap to match the localization of MZMs [76,77], since the proximity-induced superconducting pairing was introduced into the chain as a parameter and not via an interaction with a superconducting host. The localization length is one of the most important quantities that decides whether the MZMs are separated enough to be feasible for topological quantum computation. In the above context, we mention that the host-induced suppression of Majorana localization length was studied on the model level by Das Sarma *et al.* [31], which also underlines the importance of the correct treatment of the host presented in this paper.

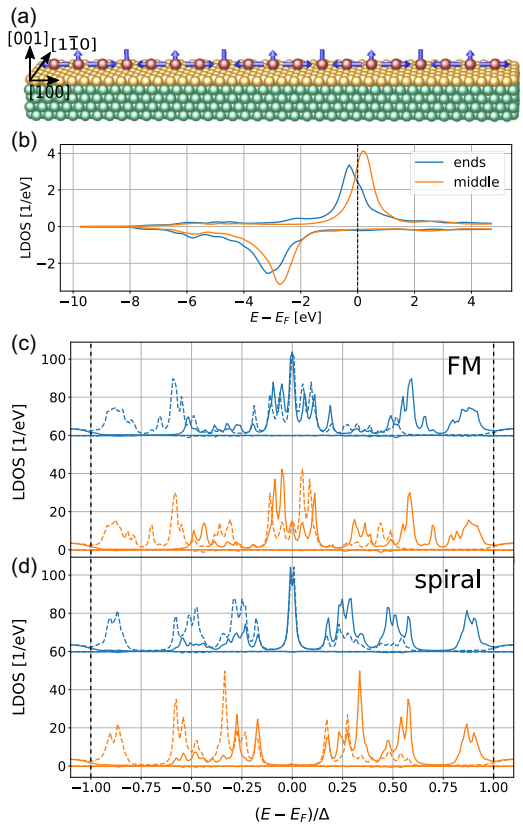


FIG. 1. The LDOS of the $2a$-[100] $Fe_{19}$ chain on Au/Nb(110) in the normal and in the superconducting state. (a) The illustration of the 19 atomic $2a$-[100] Fe chain on Nb(110) covered with a single monolayer Au; the spin configuration shows a Néel spiral with 90° spiraling angle. (b) The normal-state local density of states for the ferromagnetic chain. (c) The LDOS in the superconducting state of the ferromagnetic chain. (d) The LDOS of the same chain as in (c) but in a Néel spiral state with 90° rotation angle as shown in panel (a). In panels (c) and (d), the solid lines are electron densities, while the dashed lines are hole densities, and the blue curves are shifted 60 1/eV. In all plots, the positive values are from the minority-spin channel and the negative values are from the majority-spin channel. The blue curves are calculated on the first atom of the chain and the orange curves are from the middle of the chain. The black dashed vertical lines in panels (c) and (d) indicate the superconducting gap of the Nb, $\Delta = 1.51$ meV.

## III. SPIN SPIRALS IN THE SUPERCONDUCTING STATE

First, we discuss the results of the first-principles calculations in the normal state on the same system introduced in Ref. [65], namely a 19-atom-long Fe chain with $2a$ ($a =$ 330 pm) nearest-neighbor distance in the [100] direction as illustrated in Fig. 1(a) (in short, a $2a$-[110] $Fe_{19}$ chain), placed on the (110) surface of an epitaxial Au monolayer covering the surface of Nb(110) described in detail in Appendix A. The normal-state LDOS is presented in Fig. 1(b) for the ferromagnetic chain, with an out-of-plane magnetization. It can be seen that the majority spin channel is almost entirely filled and gives a negligible contribution to the normal-state LDOS at the Fermi level, and an overwhelming contribution comes from the minority spin channel. This fact is also expressed in the enhanced magnetic moment of about $3.8\mu_B$. Such elevated magnetic moments are typical for surface magnetic impurities. If we consider instead a 90° Néel-type spin spiral, for example [as illustrated in Fig. 1(a)], the normal-state LDOS remains mostly unchanged, as discussed in note 3 of the Supplemental Material [74]. In summary, we cannot detect any feature of the normal-state DOS that could signal the rather different behavior in the superconducting state that we find later between the ferromagnetic and the spin-spiral state.

Turning our attention to the superconducting state, first we confirm the experimental finding [65] that the size of the induced gap in an Au overlayer system with a single atomic layer of Au on the Nb(110) surface does not differ from the size of the gap in a pure Nb surface (the details are presented in note 4 of the Supplemental Material [74]). Hereafter, we consider the $2a$-[100] $Fe_{19}$ chain placed on this host system. The LDOS on some Fe impurity atoms of such a chain is plotted in Fig. 1(c) for a ferromagnetic spin configuration, where the LDOS in the superconducting state is obtained by

$$\mathrm{LDOS}(\varepsilon, n) = -\frac{1}{\pi}\mathrm{Im\,Tr}\left\{G^{nn,ab}_{Ls,L's'}(\varepsilon)\right\}. \tag{2}$$

Magnetic impurities are expected to cause in-gap states called Yu-Shiba-Rusinov (YSR) states [78–80]. In Fig. 1(c) it can be seen that in the magnetic chain the Yu-Shiba-Rusinov states of the single Fe impurity hybridize and start to form Shiba bands within the superconducting gap of the host, as was seen in the experiments [57,58], and the hybridized states occupy almost the entire energy range of the gap, including the zero energy. Although spin-orbit coupling naturally causes spin-mixing, it should be noted that all states are, yet again, from one spin channel only, even though our calculations are fully relativistic. This is not entirely surprising based on the normal-state DOS of the chains [see Fig. 1(b)] discussed previously. Most interestingly however, when we are repeating the calculation for a 90° Néel type spin spiral, the LDOS plotted in Fig. 1(d) shows the opening of an internal gap of $\Delta_{\mathrm{int}} = 0.22$ meV around zero energy within the hybridized YSR states. Moreover, one peak appears right in the middle of this minigap, exactly at zero energy—that is, at the Fermi energy—on the atoms at both ends of the chain, which shall be referred as the zero-energy peak (ZEP). In the context of scanning tunneling spectroscopy [81], these peaks are manifested in the zero bias peaks (ZBPs) observable in the differential conductance. Because these are exactly the features that are expected for a system with MZMs, it motivates us to investigate other spin spiral states via a computer experiment and look at how the MZMs and the minigap emerge as spin spiraling and SOC changes. But it has to be emphasized that even though there are states at zero energy at some spiraling angle, this does not necessarily mean that MZMs are found. As has been demonstrated before, even in the case of a single magnetic impurity on the surface of a superconducting host, it is possible to obtain a state at zero energy by imposing a canting angle [62], even though it is not possible to obtain MZMs for a single impurity. Such states are just YSR states that are accidentally shifted to zero energy as a result of the canting angle. Therefore extreme caution and further analysis are needed regarding the classification of the minigap and the

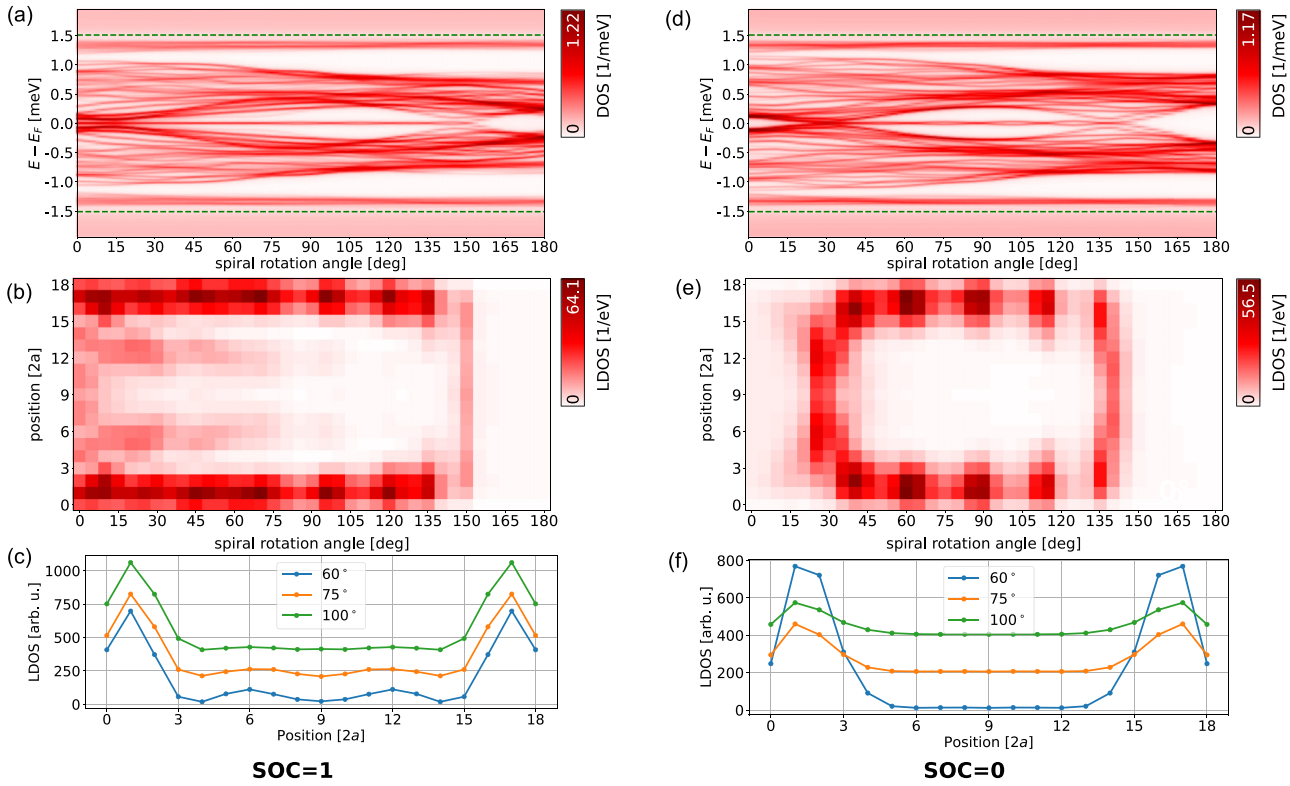


FIG. 2. The effect of the SOC on the DOS, and the localization of the ZEP of Néel spirals for the $Fe_{19}$ $2a$-[100] chains on Au/Nb(110). (a) The total DOS, including both electrons and holes, integrated along the chain plotted in the vicinity of the superconducting gap (1.51 meV), noted with green dashed lines. Calculated for Néel spirals with rotation angles changed in 5° steps between the ferromagnetic (0°) and the antiferromagnetic (180°) spin configurations, in the fully relativistic case, denoted as SOC = 1, representing the scaling factor for the SOC. (b) The electron LDOS at the Fermi energy along the $2a$-[100] $Fe_{19}$ chain on Au/Nb(110) as a function of the Néel spiral rotation angle in the fully relativistic case (SOC = 1). Parts (d) and (e) are the same as (a) and (b), but with SOC scaled to 0. In panels (c) and (f), different cross sections are shown from (b) and (e). respectively; to better show the localization of the states, the lines are plotted with an offset of 200 arb. units.

ZEPs, and in paper II in this series [82] we will show how easy it is to obtain a "fake" or quasi-Majorana state.

Based on tight-binding models [66], it is to be expected that spin spirals act along SOC to open up a minigap in the Shiba band structure. To confirm this result, we studied the effect of different spin spiral states on the formation of the ZEP and the minigap in a series of calculations for Néel-type spirals with spins rotating in the plane perpendicular to the surface ($\vec{e}_z$) and containing the chain ($\vec{e}_x$), described by the following local exchange field as $\vec{B}(i) = |\vec{B}(i)|[\sin(\theta(i-9))\vec{e}_x + \cos(\theta(i-9))\vec{e}_z]$ on site $i$. This way, the direction of the magnetic moment of the atom in the middle of the chain was fixed to point along the $z$ direction, and the neighboring spins were rotated with respect to each other with an angle $\theta$ ranging from 0° (FM) to 180° (AFM) in 5° steps.

The DOS (LDOS summed over all atoms in the chain) obtained for the different spirals as a function of the spiraling rotation angle in the fully relativistic case is shown in Fig. 2(a). Probably the most interesting feature of this figure is the existence of a peak at zero energy which is present even in the FM state and remains undisturbed all the way until about 150°. Simultaneously, we can see that there is no meaningful gap present around it in the FM case, as we noticed previously; however, as the spiraling angle is increasing, a minigap appears and increases in size from about 20°. It keeps increasing until around 110°, where it reaches its maximum value of 0.25 meV, which is 16.5% of the Nb gap. For larger spiraling angles, the minigap starts to decrease and it collapses at around 150° and then reopens again for even larger spiraling angles. While the minigap is open, from 20° to 150°, there is a zero-energy peak. However, when the gap closes and reopens at 150° this peak disappears. Such behavior is usually a signal of a topological phase transition. It should be noted that the zero-energy peak is present even for the ferromagnetic chain, where the minigap is not yet fully opened.

It was pointed out previously [47] that spin-orbit coupling plays an important role in the formation of MZMs. In our theory, it is possible to manipulate the Dirac equation in such a way that the spin-orbit coupling term is scaled out while all other relativistic effects, such as the Darwin term and the mass-velocity term, are properly taken into account [83]. To investigate the dependence of both the minigap and the ZEP on the SOC, we repeated our calculations with SOC scaled out. The results can be analyzed by comparing Figs. 2(a) and 2(d). The calculations behind these figures are completely identical otherwise. Probably the most prominent effect is that without SOC, the ferromagnetic state is gapped without a ZEP in it. When introducing a spiraling angle, this gap remains open until 40°, where it closes and reopens, however now a ZEP appears in it. The gap remains open with the ZEP

until about 135°, where the gap closes and reopens again, this time without a ZEP. Consequently, even without SOC there is a large range of spirals where a ZEP can be observed. The spiraling angles where the minigap closes and reopens also appear to be slightly different when compared to the fully relativistic case. At the points where the gap closes (and reopens), a topological phase transition is expected, as we already discussed in the fully relativistic case, where only the second transition point is present. Our results without spin-orbit coupling are quite similar to what has been described in the context of previously studied simple models of MZMs [19,20,66,67].

## IV. SPATIAL DISTRIBUTION OF THE ZERO-ENERGY PEAK

It is known even from the original work of Kitaev [84] that MZMs appear at the two ends of the chains. One should remember that the BCS pairing model leads to Cooper pairs, which are formed by electrons with opposite momenta and spins, thus mixing states from the region of the gap around the Fermi level. The coherence length is the extension of these wave packets in real space and proportional to $1/\Delta$. The frequently assumed physical picture is that the larger coherence length (smaller gap sizes) will be much more likely to cause a larger localization length and thus hybridization of MZMs [85]. The results obtained here significantly change this picture, emphasizing the importance of spin-orbit effects and material-specific treatment. To examine the spatial extent of the ZEP, we plotted the value of the local DOS (LDOS) at zero energy along all spiral atoms for Fe/Au/Nb(110) in Figs. 2(b) and 2(e), with and without SOC, respectively. Most convincingly we find that for spiraling angles where a ZEP is present, the states are localized to the atoms at the end of the chain, independently of SOC and the spiraling angle. One interesting case is the ferromagnetic Fe chain on Au/Nb(110) with SOC, where we can already see a ZEP sitting in a tiny but not perfect "gap." It is obvious from Fig. 2(b) that there are zero-energy states distributed along the entire chain, and by the introduction of a spiraling angle, the states on the in-between atoms gradually disappear, and the states finally become localized to the ends of the chain around 20°. Therefore, even in the case of the ferromagnetic chain, there is a sharp state at zero energy that continuously evolves into the end states of the gapped spirals exactly at the angle where the gap opens in Figs. 2(a) and 2(d). In the ferromagnetic state, however, because the internal gap is closed, it is masked entirely by YSR states on the in-between atoms. To better examine the formation and localization of MZMs, we repeated the plot in Figs. 2(c) and 2(f), where data from the figures above are plotted for the 60°, 75°, and 110° spirals separately. It can be seen that first of all, the extent (the localization length) of the state changes with the spiraling angle, and it is slightly different with and without SOC. Without SOC, the most delocalized state is obtained for the 110° spiral, while with SOC this appears to be the most localized one. It can also be clearly observed that with SOC, there is a small oscillatory tail to the side peaks, which overlap. Such behavior was seen in tight-binding models as well [22,85], when the MZMs on the two ends overlapped. All in all, we can conclude that the MZMs extend roughly 4 atomic positions, about 8 2D lattice constants, or 26.4 Å.

## V. THE SINGLET AND THE TRIPLET ORDER PARAMETER

In addition to the electron (and hole) densities, the KS-DBdG equations provide us with a recipe to calculate the singlet and triplet OPs. In fact, the appearance of the superconducting state is manifested in the local Green's function matrix as finite elements in the electron-hole off-diagonal block. Hence, all the order parameters related to different pairing states shall be derived based on these elements. First, we define the following LDOS-like quantity to describe the energy resolution of the spin-singlet local OP [86]:

$$\chi_S(\varepsilon, n) = -\frac{1}{\pi}\mathrm{Im}\,\mathrm{Tr}_L\,\mathcal{S}_s\left\{G^{nn,\mathrm{eh}}_{Ls,L's'}(\varepsilon)\right\}, \tag{3}$$

where $\mathrm{Tr}_L$ denotes the trace in angular-momentum space, while $\mathcal{S}_s$ generates the spin-singlet, $\mathcal{S}_s\{f(s,s')\} = \frac{\sqrt{2}}{2}(f(\frac{1}{2},-\frac{1}{2}) - f(-\frac{1}{2},\frac{1}{2}))$. The energy-resolved local singlet OP summed over the Fe atoms is shown in Figs. 3(a) and 3(d), with and without spin-orbit coupling, respectively. The singlet anomalous density shows very similar properties to the electronic DOS except for one characteristic difference, i.e., there is no ZEP. This is a property of the Bogoliubov–de Gennes theory, where the singlet OP is an odd function of the energy with respect to the zero-energy level (this is a consequence of particle-hole symmetry) and therefore it is zero at zero energy. Most nonzero energy states within the superconducting gap appear to have a nonzero OP, indicating a superconducting state. Some states, however, are such that they are entirely electronlike or holelike, which can be seen from the fact that the plot of the order parameter in Figs. 3(a) and 3(d) does not exactly match the DOS plot of Figs. 2(a) and 2(d), respectively. States that are entirely electronlike or holelike are usually regarded as normal states, where the Cooper pairs are broken. It should also be mentioned that the magnitude of the singlet OP is quite small, which most likely comes from the rather uneven normal-state density of states in spin channels which limits the formation of Cooper pairs and Andreev scattering. A larger contribution can be seen for the triplet OP, described below.

To further analyze the structure of the OP, we consider the possibility of induced spin-triplet pairing since artificially constructed heterostructures were already proven to host spin-triplet Cooper pairs [87]. Here we aim for finding the dominant component of the induced triplet OP in real space to scrutinize the behavior of the in-gap states. The fermionic nature of the electron implies that in the case of triplet pairing, the spatial component of the wave function has to be odd. In the context of a multiband Hamiltonian for bulk systems, this allows the possibility of even parity odd orbital triplet (EOT) states, which have been shown to be responsible for the experimentally observed simultaneous appearance of magnetism and superconducting state in certain materials [88,89]. In these cases, the translational invariance made it possible to introduce a proper parity operator for the whole system. However, since translational invariance is broken for surfaces and impurities, in order to avoid confusion with Refs. [89–91]

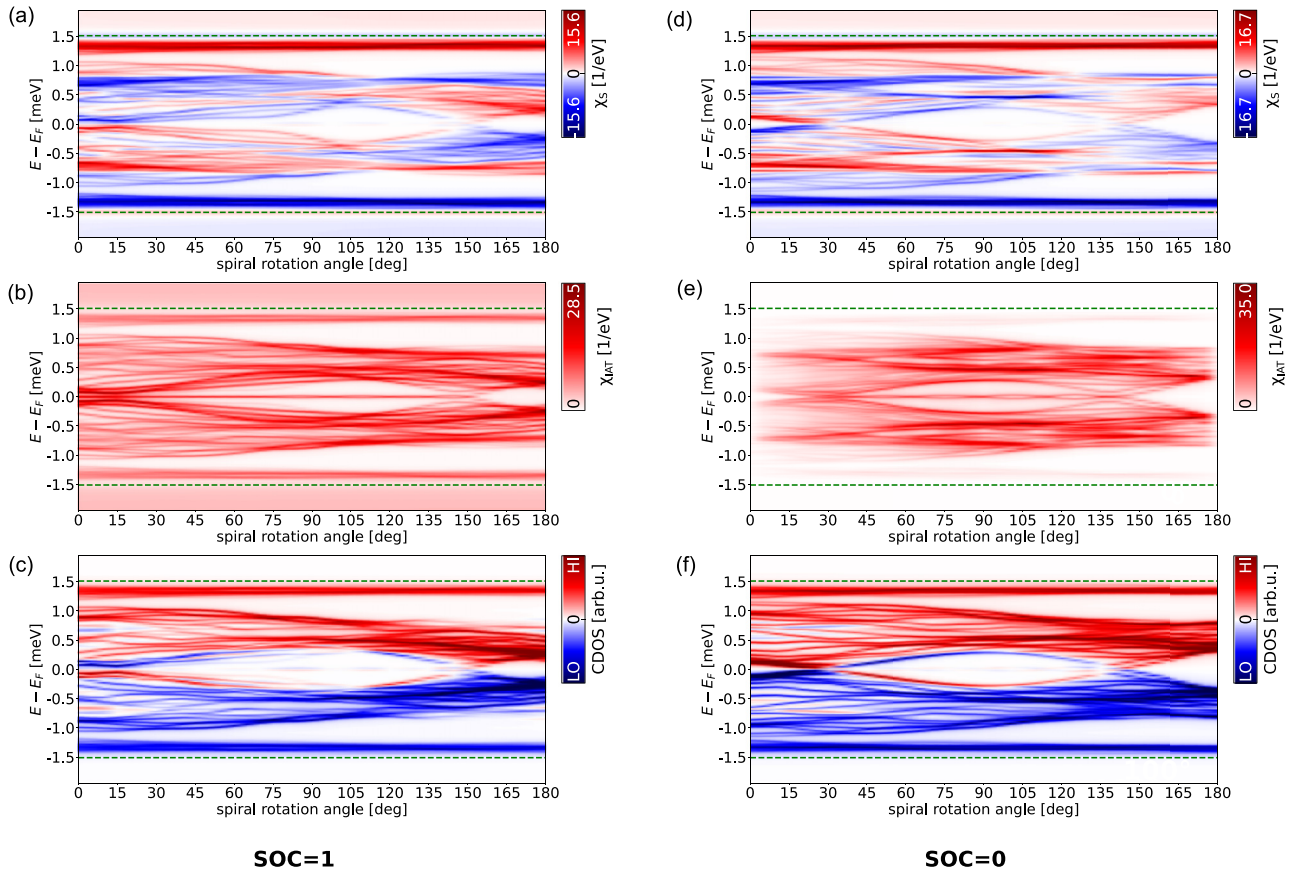


FIG. 3. The energy-resolved singlet (a),(d) and the norm of the IAT (b),(e) order parameters and the CDOS (c),(f) of Néel spirals for the $Fe_{19}$ 2*a*-[100] chains on Au/Nb(110) integrated along the chain. The green dashed lines represent the superconducting gap of Nb (1.51 meV). Calculated for Néel spirals with rotation angles changed in 5° steps between the ferromagnetic (0°) and the antiferromagnetic (180°) spin configurations. The left column shows the fully relativistic case, denoted as SOC = 1, representing the scaling factor for the SOC, while the right column shows the scalar-relativistic case, SOC = 0.

we shall adopt the term "internally antisymmetric triplet" (IAT). It is expected that the relativistic Andreev scattering process (captured accurately by the generalized multiple scattering theory for the superconducting state) yields the largest contribution for IAT which is antisymmetric with respect to the orbital degrees of freedom. The common feature behind all these concepts is that spin-orbit coupling induces triplet pairing if a singlet pairing state already exists. This statement is easy to understand within our formalism, because during the solution of the relativistic Bogoliubov–de Gennes equation, a mixing occurs between the spin and orbital degrees of freedom together with the electron-hole character. This type of symmetry classification of Cooper pairs is important since we aim to distinguish these features from the odd-frequency spin triplet pairing which may also appear in many artificial superconductor-magnet hybrid structures as presented in Ref. [40]. Therefore, we may also define a DOS-like quantity to account for the norm of the energy-resolved IAT order parameter (which is now a matrix in orbital indices):

$$\overline{\chi}_{\mathrm{IAT}}(\varepsilon) = \sum_{n} \sum_{i=-1,0,1} -\frac{1}{\pi} \left|\left|\mathrm{Im}\mathcal{A}_L \mathcal{T}_s^i \left\{G^{nn,\mathrm{eh}}_{Ls,L's'}(\varepsilon)\right\}\right|\right|_{\mathrm{F}}, \quad (4)$$

with the antisymmetrization in angular-momentum space, $\mathcal{A}_L\{f(L,L')\} = \{\frac{1}{2}[f(L,L') - f(L',L)]\}$, and the projections on spin-triplets, $\mathcal{T}_s^0\{f(s,s')\} = \frac{\sqrt{2}}{2}(f(\frac{1}{2},-\frac{1}{2}) + f(-\frac{1}{2},\frac{1}{2}))$, and $\mathcal{T}_s^{\pm 1}\{f(s,s')\} = f(\pm\frac{1}{2},\pm\frac{1}{2})$, while $||M||_{\mathrm{F}}$ denotes the Frobenius norm of matrix $M$. This quantity accounts for the emergence of IAT pairing and has been plotted in Figs. 3(b) and 3(e) with and without SOC, respectively. It can be seen that for zero SOC and for a ferromagnetic (or antiferromagnetic) configuration, the triplet OP is zero because the SOC is not inducing any mixing between the spin and the electron-hole indices. Additionally, there is a very small value of the singlet OP, and electron-hole mixing.

This is understandable and expected, based on the normal-state DOS, and it indicates that the electrons are almost entirely in the normal state. In the case of SOC at its full value, even in the ferromagnetic chain there appears to be IAT (triplet) states present. By increasing the spiraling angle, the mixing between the spin channels becomes more substantial. The magnitude of the triplet OP is an order of magnitude larger than the singlet OP for all angles. In principle, there are all types of states present: zero pairing (normal state), a small amount of singlet, and much more IAT pairing are simultaneously possible. Interestingly, a nonzero triplet OP can be seen at zero energy as well. This means that the ZEP is not only a state at zero energy, a state localized to the edge of the chain, but it is also an (IAT) triplet state.

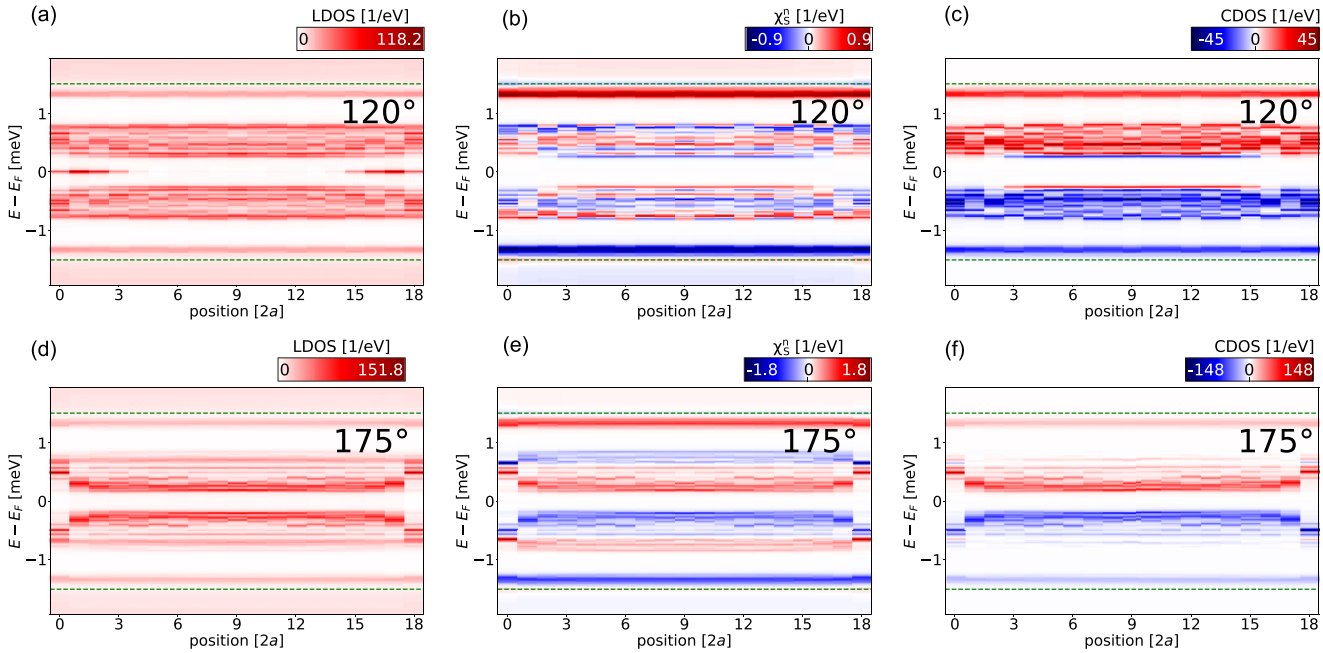


FIG. 4. The real-space structure of the LDOS and the energy-resolved singlet OP in the presence and in the absence of a ZEP. (a) The LDOS of the $2a$-[100] $Fe_{19}$ chain on Au/Nb(110) in a Néel-type spin spiral state with 120° rotation angle. (b) The energy-resolved local singlet OP $\chi_S(\varepsilon, n)$, and (c) the site-resolved CDOS of the same spiral as in (a). (d), (e), and (f) The LDOS, the $\chi_S(\varepsilon, n)$, and the site-resolved CDOS for the 175° spiral, respectively. The superconducting gap of the Nb indicated by green dashed lines. The plots include the values of the functions only for the Fe sites, while the vacuum positions in between are neglected.

## VI. TOPOLOGICAL PROPERTIES OF THE MINIGAP

Band inversion is a key signature of topological superconductivity, which can be observed if one investigates the band structure of infinite chains as a function of momenta. In finite chains it is not possible to observe band inversion in the strict definition of the term, as bands are not present. However, a real-space solution and a momentum-space solution of the KSDBdG equations for infinite chains should carry the same information, and one may expect that the signatures of band inversion—if found in a **k**-space solution—also appear in the real-space solution. Therefore, it is expected that even a finite chain may carry the signatures of topological superconductivity—provided it is long enough—which then can be obtained from a real-space calculation of the electronic states. In the superconducting state, the band inversion can be made visible by the construction of antisymmetric quantities with respect to the Fermi level. Based on the particle-hole symmetry, we found two such antisymmetric quantities which provide a clean visual picture of band inversion. One such quantity is the energy-resolved singlet OP, which is known to be antisymmetric [92] with respect to the Fermi level. As can be seen in Fig. 4, where the singlet OP is plotted, in the case of a 175° spiral, where no ZEP is present [Fig. 4(d)], the sign of the singlet OP is uniform on each atom, and the sign on either side of the minigap remains the same compared to the appropriate coherence peaks related to the bulk gap. In stark contrast, for a 120° spiral, for example, where a ZEP is present at the edge atoms of the chain [Fig. 4(a)], it changes sign prematurely along the chain and the sign of the coherence peak of the minigap is the opposite of the appropriate bulk gap's coherence peak [Fig. 4(b)], which indicates band inversion and, consequently, a topological minigap. The signatures of band inversion and the appearance of zero-energy edge states with the bulk-edge correspondence [1] can be regarded as *in silico* evidence of the existence of MZMs and topological superconductivity.

A similar visualization of the band inversion can be obtained based on the quasiparticle charge density of states (CDOS). In the superconducting state, assigning a unit charge $+e$ to the electron and $-e$ to the hole, the net quasiparticle charge density of states can be introduced as $\mathrm{CDOS}(\varepsilon) = e[\mathrm{DOS}_e(\varepsilon) - \mathrm{DOS}_h(\varepsilon)]$, where $e$ is the electron charge. Just as the density of states (DOS), the CDOS can be local to a site or summed up for all the sites in the chain.

Yet again, according to the particle-hole symmetry, the CDOS is antisymmetric with respect to the Fermi level ($\varepsilon = 0$), namely $\mathrm{CDOS}(\varepsilon) = -\mathrm{CDOS}(-\varepsilon)$. In Figs. 3(c) and 3(f) one can observe the antisymmetric property of the CDOS and it can also be concluded that in spirals, where zero-energy peaks are absent, the negative energy in-gap states have mainly electronlike character, while the positive energy in-gap states are mostly composed of holelike states. Figures 3(c) and 3(f) also illustrates that the CDOS, corresponding to the induced minigap, changes sign prematurely at the minigap edge as a function of energy, which implies that the electron-hole characters of these states are exchanged. As a function of the spiraling angle between 20° and 150°, this feature happens simultaneously with the appearance of the zero-energy state. Furthermore, the signatures of band inversion can be observed for lower spiraling angles as well, all the way to 0°, the ferromagnetic solution. This indicates that even though the

gap is filled by in-between states, as we described in Sec. IV, the state at zero energy in the ferromagnetic state is an MZM, but it is more extended and overlapping. A similar conclusion can be drawn from the singlet OP, shown in Fig. 3(a). One may also notice that neither the CDOS nor the OP shows zero-energy states due to their antisymmetric property. In Fig. 4 we explore the site-resolved local DOS (LDOS), the energy-resolved spin-singlet local OP $\chi_S(\varepsilon, n)$, and the site-resolved CDOS. The more interesting behavior can be observed on the site-resolved CDOS plot, which clearly shows that the YSR states, corresponding to the minigap, are exchanged in the internal region if the system is in the topologically nontrivial phase [Figs. 4(a)–4(c)]. Only at the edges, where MZMs appear, do the YSR states remain intact (no exchange of YSR states can be observed). We can arrive at a rather similar conclusion by studying Fig. 4(b). In fact, this process of transforming the internal "twisted" YSR states into the "untwisted" YSR states at the edges gives rise to the emergence of zero-energy edge states. Altogether, these features are clear indications of band inversion and, consequently, a topological minigap for the spiraling angles where the zero-energy states are observed at the ends of the $Fe_{19}$ chain. Therefore, from this point on, they can be called Majorana zero modes due to the bulk-edge correspondence principle [1].

Another intriguing finding in Figs. 3(b) and 3(c) (as the CDOS demonstrates around 20° in the fully relativistic case) is that the gap closing and opening with the continuous change in spiraling angles may not necessarily imply a change in the topological behavior as well. Such a change is usually considered as a rule of thumb in identifying topological superconductivity during experimental realizations. On the other hand, there can be several reasons behind this observation, including that a complicated multiband system with SOC behaves differently from model predictions [89,93], or the gap closing can cause the emergence of additional MZMs with an even number [25,30,68], or the gap does not completely close but only tightens, or this occurs for a finite (and insufficiently large) chain.

In general, the verification of topological superconductivity in experiments is a task of great importance. One possible way to connect our findings to experiments can happen through the so-called Bogoliubov-angle (the relative weight of particle and hole amplitudes in the quasiparticles). According to Ref. [94], it is a measurable quantity using STM, and it can be measured locally by comparing the ratios of tunneling currents at positive and negative biases [94]. Therefore, the energy and position-dependent electron-hole character can be extracted from the STM measurements, which allows the construction of a suitable quantity that obeys similar properties to the site-resolved charge density of states (antisymmetric in energy with respect to the Fermi level). The measurement of this type of antisymmetric quantities can support the experimental validation of the topological nature of experimentally observed zero bias peaks. Furthermore, we mention that the relative weight of the particle and hole amplitude of the quasiparticle can also be measured with angular resolved photoemission spectroscopy (ARPES) [95], allowing to achieve momentum space resolution. Therefore, this idea can be generalized for investigations of bulk topological superconductors as well, where band inversion should be observable in momentum space. On the other hand, further research is needed in the exact formulation of such a quantity that is optimally tuned to STM experiments.

## VII. CONCLUSIONS

To summarize, using a first-principles-based solution to the Dirac-Bogoliubov–de Gennes equations, we studied linear chains of Fe atoms placed on the surface of Au-covered Nb(110) in the superconducting state. We found that (i) in agreement with experiments, a ferromagnetic state does not support a minigap around zero energy; (ii) in a spin spiral state, however, a minigap emerges at about a 20-deg spiraling angle with a spin-polarized zero energy state in it. This state bears all the signatures of being an MZM. It is localized to the two ends of the chain, it is a spin triplet state, and it is in a topological gap. At larger spiraling angles, the gap closes. (iii) We also showed that this state extends to about four to five atoms, and they more easily overlap in the presence of spin-orbit coupling. (iv) Moreover, our calculations revealed that the MZMs bear the characteristic feature of nonunitary internally antisymmetric triplet states, which are thought to be responsible for time-reversal symmetry breaking in a large class of bulk superconductors [90]. (v) We have also proposed that site-resolved quantities, which are antisymmetric in energy with respect to the Fermi level, show band inversion and can serve as an identification of the topological phase. We made quantitative predictions for the superconducting (singlet) order parameter and the charge density of states, which fulfills this requirement of antisymmetric behavior. Moreover, analogous conductance-based quantities can be constructed which can be measurable with scanning tunneling microscopy (STM) [94].

In part II of our investigations, we will show that the Majorana Zero Mode we found in the present paper, is quite robust against various perturbations of the magnetic state. We will also explore potential routes to non-topological zero energy edge states, and combine different spin spirals to shed light on other fascinating - and potentially quite useful - phenomena: the shift of MZMs with changing spiraling angles and topological fragmentation as a result of phase shifts on the chain.

## ACKNOWLEDGMENTS

B.N., L.A., L.S., and B.U. acknowledge financial support by the National Research, Development, and Innovation Office (NRDI Office) of Hungary under Projects No. FK124100, No. K131938, and No. K142652. B.N. and L.S. acknowledge support by the Ministry of Culture and Innovation and the NRDI Office within the Quantum Information National Laboratory of Hungary (Grant No. 2022-2.1.1-NL-2022-00004). B.N. acknowledges the support by the ÊNKP-22-4-I New National Excellence Program of the Ministry of Culture and Innovation from the source of the NRDI Fund. The authors acknowledge KIFÌ for awarding us access to resources based in Hungary.

## APPENDIX

### 1. The details of first-principles calculations

As we mentioned in Sec. II, following Ref. [72] the KSDBdG equations shall be solved self-consistently by assuming that the superconducting host has isotropic *s*-wave spin-singlet pairing as described by BCS theory [73]. Such a solution results in self-consistent charge and magnetization density and effective pairing potential. However, since the small superconducting gap is not likely to cause large modifications in the charge and magnetization density, and consequently in the atomic potentials, in this paper we followed the usual approximation [96] for the effective pairing potential $\Delta_{\text{eff}}(\vec{r})$, meaning that this quantity is fitted to the experimental value of the superconducting bulk gap of the Nb host, and zero otherwise, without requiring self-consistency for $\Delta_{\text{eff}}$ while self-consistency is maintained in the charge and magnetization density. Furthermore, in this work, we imposed various spin spirals on the direction of the magnetic moments of the atoms in the nanowire deposited on the surface of an *s*-wave superconductor. The calculations were performed in terms of the screened Korringa-Kohn-Rostoker method (SKKR), based on a fully relativistic Green's function formalism by solving the Dirac equation for the normal state [97] and the Kohn-Sham-Dirac-Bogoliubov–de Gennes (KSD-BdG) equation for the superconducting state within multiple scattering theory (MST) [59,60,96]. The chains are included within an embedding scheme [98], being an efficient method to address the electronic and magnetic properties or the in-gap spectra of real-space atomic structures without introducing a supercell. In calculations for the Fe/Au/Nb(110) system consist of seven atomic layers of Nb, a single atomic layer of Au, and four atomic layers of vacuum between semi-infinite bulk Nb and semi-infinite vacuum. The Fe impurities are placed in the hollow position in the vacuum above the Au layer and relaxed towards the surface by 21%, while the top Au layer is also relaxed inwards by 2%. The relaxations are obtained from total-energy minimization in a VASP [99–101] calculation for a single Fe adatom, and they are used in all of the calculations. For the potentials we employ the atomic sphere approximation (ASA), while the normal state is calculated self-consistently in the local density approximation (LDA) as parametrized by Vosko *et al.* [102]. The partial waves within MST are treated with an angular momentum cutoff of $\ell_{\max} = 2$. In the self-consistent normal state calculations, we used a Brillouin zone (BZ) integration with 253 **k** points in the irreducible wedge of the BZ and a semicircular energy contour on the upper complex plane with 16 points for energy integration. To take into account charge relaxation around the magnetic sites, the atomic chains are calculated with a neighborhood corresponding to two atomic shells or a spherical radius of $r = 1.01a$ around the Fe atoms. This way the atomic cluster used for embedding the $Fe_{19}$ chain contained 339 atomic sites altogether. After having obtained the self-consistent potentials in the normal state, quantities in the superconducting state were calculated by a single-shot calculation by solving the KSDBdG equation with the experimental band gap $\Delta = 1.51$ meV [45] used as the pairing potential in the Nb layers [60]. The BZ integration for the host Green's function was performed by using an increasing number of **k** points with respect to the normal state, including 1891 points in the irreducible wedge of the BZ. A sufficient energy resolution of the LDOS in the superconducting gap is acquired by considering 301 energy points between $\pm 1.95$ meV with an imaginary part of 13.6 μeV related to the smearing of the resulting LDOS.


[1] X.-L. Qi and S.-C. Zhang, Rev. Mod. Phys. **83**, 1057 (2011).
[2] M. Sato and Y. Ando, Rep. Prog. Phys. **80**, 076501 (2017).
[3] L. A. Wray, S.-Y. Xu, Y. Xia, Y. S. Hor, D. Qian, A. V. Fedorov, H. Lin, A. Bansil, R. J. Cava, and M. Z. Hasan, Nat. Phys. **6**, 855 (2010).
[4] S. Sasaki, M. Kriener, K. Segawa, K. Yada, Y. Tanaka, M. Sato, and Y. Ando, Phys. Rev. Lett. **107**, 217001 (2011).
[5] Y. Ueno, A. Yamakage, Y. Tanaka, and M. Sato, Phys. Rev. Lett. **111**, 087002 (2013).
[6] P. Zhang, K. Yaji, T. Hashimoto, Y. Ota, T. Kondo, K. Okazaki, Z. Wang, J. Wen, G. D. Gu, H. Ding, and S. Shin, Science **360**, 182 (2018).
[7] S. Ran, C. Eckberg, Q.-P. Ding, Y. Furukawa, T. Metz, S. R. Saha, I.-L. Liu, M. Zic, H. Kim, J. Paglione, and N. P. Butch, Science **365**, 684 (2019).
[8] K.-H. Jin, H. Huang, J.-W. Mei, Z. Liu, L.-K. Lim, and F. Liu, npj Comput. Mater. **5**, 57 (2019).
[9] K. E. Avers, W. J. Gannon, S. J. Kuhn, W. P. Halperin, J. A. Sauls, L. DeBeer-Schmitt, C. D. Dewhurst, J. Gavilano, G. Nagy, U. Gasser, and M. R. Eskildsen, Nat. Phys. **16**, 531 (2020).
[10] L. Jiao, S. Howard, S. Ran, Z. Wang, J. O. Rodriguez, M. Sigrist, Z. Wang, N. P. Butch, and V. Madhavan, Nature (London) **579**, 523 (2020).
[11] Y. W. Li, H. J. Zheng, Y. Q. Fang, D. Q. Zhang, Y. J. Chen, C. Chen, A. J. Liang, W. J. Shi, D. Pei, L. X. Xu, S. Liu, J. Pan, D. H. Lu, M. Hashimoto, A. Barinov, S. W. Jung, C. Cacho, M. X. Wang, Y. He, L. Fu *et al.*, Nat. Commun. **12**, 2874 (2021).
[12] J. R. Badger, Y. Quan, M. C. Staab, S. Sumita, A. Rossi, K. P. Devlin, K. Neubauer, D. S. Shulman, J. C. Fettinger, P. Klavins, S. M. Kauzlarich, D. Aoki, I. M. Vishik, W. E. Pickett, and V. Taufour, Commun. Phys. **5**, 22 (2022).
[13] L. Fu and C. L. Kane, Phys. Rev. Lett. **100**, 096407 (2008).
[14] R. M. Lutchyn, J. D. Sau, and S. Das Sarma, Phys. Rev. Lett. **105**, 077001 (2010).
[15] Y. Oreg, G. Refael, and F. von Oppen, Phys. Rev. Lett. **105**, 177002 (2010).
[16] T.-P. Choy, J. M. Edge, A. R. Akhmerov, and C. W. J. Beenakker, Phys. Rev. B **84**, 195442 (2011).
[17] V. Mourik, K. Zuo, S. M. Frolov, S. R. Plissard, E. P. A. M. Bakkers, and L. P. Kouwenhoven, Science **336**, 1003 (2012).
[18] M. Kjaergaard, K. Wölms, and K. Flensberg, Phys. Rev. B **85**, 020503(R) (2012).
[19] I. Martin and A. F. Morpurgo, Phys. Rev. B **85**, 144505 (2012).
[20] S. Nadj-Perge, I. K. Drozdov, B. A. Bernevig, and A. Yazdani, Phys. Rev. B **88**, 020407(R) (2013).

[21] J. Klinovaja, P. Stano, A. Yazdani, and D. Loss, Phys. Rev. Lett. **111**, 186805 (2013).
[22] D. Rainis, L. Trifunovic, J. Klinovaja, and D. Loss, Phys. Rev. B **87**, 024515 (2013).
[23] M. M. Vazifeh and M. Franz, Phys. Rev. Lett. **111**, 206802 (2013).
[24] S. Nakosai, Y. Tanaka, and N. Nagaosa, Phys. Rev. B **88**, 180503(R) (2013).
[25] J. Li, H. Chen, I. K. Drozdov, A. Yazdani, B. A. Bernevig, and A. H. MacDonald, Phys. Rev. B **90**, 235433 (2014).
[26] A. Heimes, P. Kotetes, and G. Schön, Phys. Rev. B **90**, 060507(R) (2014).
[27] S. Nadj-Perge, I. K. Drozdov, J. Li, H. Chen, S. Jeon, J. Seo, A. H. MacDonald, B. A. Bernevig, and A. Yazdani, Science **346**, 602 (2014).
[28] M. Ruby, F. Pientka, Y. Peng, F. von Oppen, B. W. Heinrich, and K. J. Franke, Phys. Rev. Lett. **115**, 197204 (2015).
[29] H.-Y. Hui, P. Brydon, J. D. Sau, S. Tewari, and S. D. Sarma, Sci. Rep. **5**, 8880 (2015).
[30] E. Dumitrescu, B. Roberts, S. Tewari, J. D. Sau, and S. Das Sarma, Phys. Rev. B **91**, 094505 (2015).
[31] S. D. Sarma, H.-Y. Hui, P. M. R. Brydon, and J. D. Sau, New J. Phys. **17**, 075001 (2015).
[32] Y. Peng, F. Pientka, L. I. Glazman, and F. von Oppen, Phys. Rev. Lett. **114**, 106801 (2015).
[33] M. H. Christensen, M. Schecter, K. Flensberg, B. M. Andersen, and J. Paaske, Phys. Rev. B **94**, 144509 (2016).
[34] G. L. Fatin, A. Matos-Abiague, B. Scharf, and I. Žutić, Phys. Rev. Lett. **117**, 077002 (2016).
[35] J. Li, T. Neupert, B. A. Bernevig, and A. Yazdani, Nat. Commun. **7**, 10395 (2016).
[36] M. T. Deng, S. Vaitiekėnas, E. B. Hansen, J. Danon, M. Leijnse, K. Flensberg, J. Nygård, P. Krogstrup, and C. M. Marcus, Science **354**, 1557 (2016).
[37] M. Hell, M. Leijnse, and K. Flensberg, Phys. Rev. Lett. **118**, 107701 (2017).
[38] P. Marra and M. Cuoco, Phys. Rev. B **95**, 140504(R) (2017).
[39] M. Mashkoori, S. Pradhan, K. Björnson, J. Fransson, and A. M. Black-Schaffer, Phys. Rev. B **102**, 104501 (2020).
[40] J. Cayao, C. Triola, and A. M. Black-Schaffer, Eur. Phys. J.: Spec. Top. **229**, 545 (2020).
[41] C. J. F. Carroll and B. Braunecker, Phys. Rev. B **104**, 245133 (2021).
[42] C. J. F. Carroll and B. Braunecker, Phys. Rev. B **104**, 245134 (2021).
[43] J. Cayao and A. M. Black-Schaffer, Phys. Rev. B **104**, L020501 (2021).
[44] K. Flensberg, F. von Oppen, and A. Stern, Nat. Rev. Mater. **6**, 944 (2021).
[45] P. Beck, L. Schneider, L. Rózsa, K. Palotás, A. Lászlóffy, L. Szunyogh, J. Wiebe, and R. Wiesendanger, Nat. Commun. **12**, 2040 (2021).
[46] P. Marra, D. Inotani, and M. Nitta, Phys. Rev. B **105**, 214525 (2022).
[47] P. Marra, J. Appl. Phys. **132**, 231101 (2022).
[48] U. Güngördü and A. A. Kovalev, J. Appl. Phys. **132**, 041101 (2022).
[49] D. Steffensen, M. H. Christensen, B. M. Andersen, and P. Kotetes, Phys. Rev. Res. **4**, 013225 (2022).
[50] J. Neuhaus-Steinmetz, E. Y. Vedmedenko, T. Posske, and R. Wiesendanger, Phys. Rev. B **105**, 165415 (2022).
[51] D. Crawford, E. Mascot, M. Shimizu, R. Wiesendanger, D. K. Morr, H. O. Jeschke, and S. Rachel, Phys. Rev. B **107**, 075410 (2023).
[52] C. Nayak, S. H. Simon, A. Stern, M. Freedman, and S. Das Sarma, Rev. Mod. Phys. **80**, 1083 (2008).
[53] J. Alicea, Rep. Prog. Phys. **75**, 076501 (2012).
[54] C. W. J. Beenakker, SciPost Phys. Lect. Notes 15 (2020).
[55] S. Jeon, Y. Xie, J. Li, Z. Wang, B. A. Bernevig, and A. Yazdani, Science **358**, 772 (2017).
[56] H. Kim, A. Palacio-Morales, T. Posske, L. Rózsa, K. Palotás, L. Szunyogh, M. Thorwart, and R. Wiesendanger, Sci. Adv. **4**, eaar5251 (2018).
[57] L. Schneider, P. Beck, T. Posske, D. Crawford, E. Mascot, S. Rachel, R. Wiesendanger, and J. Wiebe, Nat. Phys. **17**, 943 (2021).
[58] L. Schneider, P. Beck, J. Neuhaus-Steinmetz, L. Rózsa, T. Posske, J. Wiebe, and R. Wiesendanger, Nat. Nanotechnol. **17**, 384 (2022).
[59] G. Csire, A. Deák, B. Nyári, H. Ebert, J. F. Annett, and B. Újfalussy, Phys. Rev. B **97**, 024514 (2018).
[60] B. Nyári, A. Lászlóffy, L. Szunyogh, G. Csire, K. Park, and B. Ujfalussy, Phys. Rev. B **104**, 235426 (2021).
[61] T. G. Saunderson, J. F. Annett, G. Csire, and M. Gradhand, Phys. Rev. B **105**, 014424 (2022).
[62] K. Park, B. Nyari, A. Laszloffy, L. Szunyogh, and B. Ujfalussy, New J. Phys. **25**, 033022 (2023).
[63] M.-H. Wu, E. Thill, J. Crosbie, T. G. Saunderson, and M. Gradhand, Phys. Rev. B **107**, 094409 (2023).
[64] A. Linscheid, A. Sanna, F. Essenberger, and E. K. U. Gross, Phys. Rev. B **92**, 024505 (2015).
[65] P. Beck, B. Nyari, L. Schneider, L. Rozsa, A. Laszloffy, K. Palotas, L. Szunyogh, B. Ujfalussy, J. Wiebe, and R. Wiesendanger, Commun. Phys. **6**, 83 (2023).
[66] F. Pientka, L. I. Glazman, and F. von Oppen, Phys. Rev. B **88**, 155420 (2013).
[67] F. Pientka, Y. Peng, L. Glazman, and F. von Oppen, Phys. Scr. **T164**, 014008 (2015).
[68] A. Heimes, D. Mendler, and P. Kotetes, New J. Phys. **17**, 023051 (2015).
[69] J. Alicea, Y. Oreg, G. Refael, F. von Oppen, and M. P. A. Fisher, Nat. Phys. **7**, 412 (2011).
[70] K. Pöyhönen, A. Weststrom, J. Röntynen, and T. Ojanen, Phys. Rev. B **89**, 115109 (2014).
[71] P. M. R. Brydon, S. Das Sarma, H.-Y. Hui, and J. D. Sau, Phys. Rev. B **91**, 064505 (2015).
[72] L. N. Oliveira, E. K. U. Gross, and W. Kohn, Phys. Rev. Lett. **60**, 2430 (1988).
[73] J. Bardeen, L. N. Cooper, and J. R. Schrieffer, Phys. Rev. **108**, 1175 (1957).
[74] See Supplemental Material at http://link.aps.org/supplemental/10.1103/PhysRevB.108.134512 for details of the first-principles based treatment of artificial superconducting heterostructures (Note 1), the computational procedure (Note 2), the normal-state LDOS compared between the FM and a 90° spiral state (Note 3), the superconducting DOS of the Au/Nb(110) layered system (Note 4), and the superconducting LDOS as a function of SOC (Note 5). The Supplemental Material also contains Refs. [103–108].

[75] J. Minár, O. Šipr, J. Braun, and H. Ebert, in *Springer Proceedings in Physics* (Springer, Cham, 2018), pp. 93–142.
[76] L. Schneider, S. Brinker, M. Steinbrecher, J. Hermenau, T. Posske, M. dos Santos Dias, S. Lounis, R. Wiesendanger, and J. Wiebe, Nat. Commun. **11**, 4707 (2020).
[77] D. Crawford, E. Mascot, M. Shimizu, P. Beck, J. Wiebe, R. Wiesendanger, H. O. Jeschke, D. K. Morr, and S. Rachel, npj Quantum Mater. **7**, 117 (2022).
[78] L. Yu, Acta Phys. Sin. **21**, 75 (1965).
[79] H. Shiba, Prog. Theor. Phys. **40**, 435 (1968).
[80] A. I. Rusinov, Zh. Eksp, Teor. Fiz. Pisma Red. **9**, 146 (1968) [JETP Lett. **9**, 85 (1969)].
[81] D.-J. Choi, N. Lorente, J. Wiebe, K. von Bergmann, A. F. Otte, and A. J. Heinrich, Rev. Mod. Phys. **91**, 041001 (2019).
[82] A. Lászlóffy, B. Nyári, G. Csire, L. Szunyogh, and B. Újfalussy, following paper, Phys. Rev. B **108**, 134513 (2023).
[83] H. Ebert, H. Freyer, A. Vernes, and G.-Y. Guo, Phys. Rev. B **53**, 7721 (1996).
[84] A. Y. Kitaev, Phys. Usp. **44**, 131 (2001).
[85] C. Fleckenstein, F. Domínguez, N. Traverso Ziani, and B. Trauzettel, Phys. Rev. B **97**, 155425 (2018).
[86] G. Csire, J. Cserti, and B. Újfalussy, J. Phys.: Condens. Matter **28**, 495701 (2016).
[87] J. W. A. Robinson, J. D. S. Witt, and M. G. Blamire, Science **329**, 59 (2010).
[88] S. K. Ghosh, G. Csire, P. Whittlesea, J. F. Annett, M. Gradhand, B. Újfalussy, and J. Quintanilla, Phys. Rev. B **101**, 100506(R) (2020).
[89] G. Csire, J. F. Annett, J. Quintanilla, and B. Újfalussy, Phys. Rev. B **106**, L020501 (2022).
[90] S. K. Ghosh, M. Smidman, T. Shang, J. F. Annett, A. D. Hillier, J. Quintanilla, and H. Yuan, J. Phys.: Condens. Matter **33**, 033001 (2021).
[91] G. Csire, B. Újfalussy, and J. F. Annett, Eur. Phys. J. B **91**, 217 (2018).
[92] J. B. Ketterson and S. N. Song, *Superconductivity* (Cambridge University Press, Cambridge, 1999).
[93] A. Ramires, J. Phys.: Condens. Matter **34**, 304001 (2022).
[94] K. Fujita, I. Grigorenko, J. Lee, W. Wang, J. X. Zhu, J. C. Davis, H. Eisaki, S. Uchida, and A. V. Balatsky, Phys. Rev. B **78**, 054510 (2008).
[95] A. V. Balatsky, W. S. Lee, and Z. X. Shen, Phys. Rev. B **79**, 020505(R) (2009).
[96] G. Csire, B. Újfalussy, J. Cserti, and B. Győrffy, Phys. Rev. B **91**, 165142 (2015).
[97] L. Szunyogh, B. Újfalussy, and P. Weinberger, Phys. Rev. B **51**, 9552 (1995).
[98] B. Lazarovits, L. Szunyogh, and P. Weinberger, Phys. Rev. B **65**, 104441 (2002).
[99] G. Kresse and J. Furthmüller, Comput. Mater. Sci. **6**, 15 (1996).
[100] G. Kresse and J. Furthmüller, Phys. Rev. B **54**, 11169 (1996).
[101] J. Hafner, J. Comput. Chem. **29**, 2044 (2008).
[102] S. H. Vosko, L. Wilk, and M. Nusair, Can. J. Phys. **58**, 1200 (1980).
[103] K. Capelle and E. K. U. Gross, Phys. Rev. B **59**, 7140 (1999).
[104] K. Capelle and E. K. U. Gross, Phys. Rev. B **59**, 7155 (1999).
[105] P. Rüßmann and S. Blügel, Phys. Rev. B **105**, 125143 (2022).
[106] R. Zeller, P. H. Dederichs, B. Újfalussy, L. Szunyogh, and P. Weinberger, Phys. Rev. B **52**, 8807 (1995).
[107] L. Szunyogh, B. Újfalussy, P. Weinberger, and J. Kollár, Phys. Rev. B **49**, 2721 (1994).
[108] M. B. Suvasini, W. M. Temmerman, and B. L. Gyorffy, Phys. Rev. B **48**, 1202 (1993).